American Mineralogist, Volume 107, pages 110–115, 2022

High-pressure experimental study of tetragonal $CaSiO_3$-perovskite to 200 GPa

Ningyu Sun[1,2], Hui Bian[1], Youyue Zhang[1], Jung-Fu Lin[3], Vitali B. Prakapenka[4], and Zhu Mao[1,2,*]

[1]Laboratory of Seismology and Physics of Earth's Interior, School of Earth and Planetary Sciences, University of Science and Technology of China, Hefei, Anhui 230026, China
[2]CAS Center for Excellence in Comparative Planetology, University of Science and Technology of China, Hefei, Anhui 230026, China
[3]Department of Geological Sciences, Jackson School of Geosciences, The University of Texas at Austin, Austin, Texas 78712, U.S.A.
[4]Center for Advanced Radiation Sources, University of Chicago, Chicago, Illinois 60637, U.S.A.

Abstract

In this study, we have investigated the crystal structure and equation of state of tetragonal $CaSiO_3$-perovskite up to 200 GPa using synchrotron X-ray diffraction in laser-heated diamond-anvil cells. X-ray diffraction patterns of the quenched $CaSiO_3$-perovskite above 148 GPa clearly show that 200, 211, and 220 peaks of the cubic phase split into 004+220, 204+312, and 224+400 peak pairs, respectively, in the tetragonal structure, and their calculated full-width at half maximum (FWHM) exhibits a substantial increase with pressure. The distribution of diffraction peaks suggests that the tetragonal $CaSiO_3$-perovskite most likely has an *I*4/*mcm* space group at 300 K between 148 and 199 GPa, although other possibilities might still exist. Using the Birch-Murnaghan equations, we have determined the equation of state of tetragonal $CaSiO_3$-perovskite, yielding the bulk modulus K_{0T} = 227(21) GPa with the pressure derivative of the bulk modulus, K'_{0T} = 4.0(3). Modeled sound velocities at 580 K and around 50 GPa using our results and literature values show the difference in the compressional (V_P) and shear-wave velocity (V_S) between the tetragonal and cubic phases to be 5.3 and 6.7%, respectively. At ~110 GPa and 1000 K, this phase transition leads to a 4.3 and 9.1% jump in V_P and V_S, respectively. Since the addition of Ti can elevate the transition temperature, the transition from the tetragonal to cubic phase may have a seismic signature compatible with the observed mid-lower mantle discontinuity around the cold subduction slabs, which needs to be explored in future studies.

Keywords: Tetragonal $CaSiO_3$-perovskite, equation of state, crystal structure, high pressure

Introduction

$CaSiO_3$-perovskite is one of the most abundant silicate phases and the dominant host of Ca in the Earth's lower mantle (Anderson 1989; Kesson et al. 1998; Murakami et al. 2005; Ringwood 1975). In the lower mantle, the volume percentage of $CaSiO_3$-perovskite is estimated to be 5–8% but could be up to 22–29% in the subducting mid-ocean ridge basalts (MORBs) (e.g., Anderson 1989; Harte 2010; Hirose et al. 2005; Wood 2000). Recent high-pressure studies have found that the shear-wave velocity of $CaSiO_3$-perovskite is substantially lower than the global seismic model PREM (Dziewonski and Anderson 1981; Gréaux et al. 2019; Kawai and Tsuchiya 2014; Thomson et al. 2019). Enrichment of the recycled MORBs with the low-velocity $CaSiO_3$-perovskite could cause a seismic signature compatible with the large-low shear velocity provinces (Thomson et al. 2019). Experimental studies on the structure and elastic properties of $CaSiO_3$ at high pressures are thus important to understand the composition and structure of the lower mantle (e.g., Komabayashi et al. 2007; Kurashina et al. 2004; Mao et al. 1989; Noguchi et al. 2013; Shim et al. 2000; Sun et al. 2016; Wang et al. 1996; Wood 2000; Zhang et al. 2006).

$CaSiO_3$-perovskite has been reported to crystallize in a cubic structure ($Pm\bar{3}m$) at the expected pressure-temperature conditions of the lower mantle (e.g., Komabayashi et al. 2007; Noguchi et al. 2013; Shim et al. 2000; Sun et al. 2016). However, it can also accommodate a certain amount of minor elements such as Ti (Hirose and Fei 2002; Kesson et al. 1998, 1994; Nestola et al. 2018; Wood 2000), which can elevate the phase transition temperature at lower-mantle pressures and may enable the tetragonal phase to exist in the cold subducting slabs (Kurashina et al. 2004; Thomson et al. 2019). The cubic to tetragonal phase transition with the presence of Ti, which is likely to happen beyond 1000 km depth may explain the observed seismic reflections in the mid-lower mantle (Kudo et al. 2012; Thomson et al. 2019).

In contrast to the cubic phase, the crystal structure and equation of state (EoS) of tetragonal $CaSiO_3$-perovskite were not well constrained. The cubic to tetragonal phase transition was proposed to be caused by a second-order structure distortion, and four space groups, including *P*4/*mmm*, *P*4/*mbm*, *I*4/*mmm*, and *I*4/*mcm* were proposed for the tetragonal phase (Shim et al. 2002; Stixrude et al. 2007). The occurrence of two potential structures (*P*4/*mbm* and *I*4/*mcm*) can be explained by the octahedral rotations, whereas the *P*4/*mmm* structure could be formed by elongating the *c*-axis of the cubic phase (Shim et al. 2002; Stixrude et al. 2007). Slightly shifting the oxygen position of the cubic phase can change the structure to tetragonal *I*4/*mmm*. In early experimental studies,

* E-mail: zhumao@ustc.edu.cn

0003-004X/22/0001–110$05.00/DOI: https://doi.org/10.2138/am-2021-7913

the *P*4/*mmm* model was applied to analyze the lattice parameters and unit-cell volume of tetragonal $CaSiO_3$, yielding a modified *c*/*a* ratio (*Z* = 1) of 0.992–0.998 at 0–100 GPa (Ono et al. 2004; Shim et al. 2002). However, theoretical studies showed that the phase transition is second order in nature and should be caused by octahedral rotations (Stixrude et al. 1996, 2007). *I*4/*mcm* with the lowest calculated energy is theoretically supported to be the stable structure for the tetragonal $CaSiO_3$ (Stixrude et al. 2007). In contrast to *P*4/*mmm*, *I*4/*mcm* has a modified *c*/*a* ratio that increases from 1.004 at 20 GPa to 1.023 at ~220 GPa (Jung and Oganov 2005; Stixrude et al. 2007). *I*4/*mcm* was also preferred in a recent experimental study based on the Rietveld refinement results, which give better fits for the peak positions and intensities than other proposed space groups (Chen et al. 2018). Meanwhile, a few theoretical studies using first-principle calculations also suggested an orthorhombic structure for $CaSiO_3$ at high pressures and low temperatures (Akber-Knutson et al. 2002; Li et al. 2006; Magyari- Köpe et al. 2002). In addition, the bulk modulus of tetragonal $CaSiO_3$-perovskite is highly uncertain, ranging from 223(6) to 248(8) GPa with a fixed pressure derivative of the bulk modulus at 4 (Chen et al. 2018; Gréaux et al. 2019; Ono et al. 2004; Shim et al. 2002; Thomson et al. 2019). The structure and EoS of tetragonal $CaSiO_3$-perovskite at high pressures thus require further investigation.

In this study, we investigated the structure of $CaSiO_3$-perovskite using synchrotron X-ray diffraction in laser-heated diamond-anvil cells (DACs). Our study has significantly extended the experimental pressure to 200 GPa. High-resolution XRD data allow us to provide direct constraints on the crystal structure, lattice parameters, and EoS of the tetragonal phase. These results have allowed for a comprehensive understanding on the structure and EoS of tetragonal $CaSiO_3$-perovskite at high pressures.

Experimental methods

The starting material was $CaSiO_3$ wollastonite, purchased from Sigma-Aldrich Co. LLC, with purity of 99%. The polycrystalline starting material was ground into fine powder and mixed with 5 wt% Pt as the pressure standard and laser absorber (Fei et al. 2007). The sample mixture was compressed by a DAC into ~10 μm thick pellets. We further cut the sample foil into small pieces. A small sample piece was sandwiched between two NaCl layers, which were pre-loaded to each side of the DAC. NaCl used as the pressure medium and thermal insulator was pre-dried for more than 5 h at ~105 °C to avoid any potential contamination of water in the air. The sample sandwiches were loaded into symmetric DACs with 75/300 μm beveled diamonds anvils. The high-pressure and -temperature XRD experiments were performed at the GeoSoilEnviroConsortium (GSECARS) of the Advanced Photon Source (APS), Argonne National Laboratory (ANL), with an X-ray wavelength of 0.3344 Å. Previous studies have shown that cubic $CaSiO_3$-perovskite is stable up to 156 GPa and will transform into a tetragonal phase after quench (e.g., Noguchi et al. 2013; Shim et al. 2000; Sun et al. 2016). Here we directly compressed the cell to ~160 GPa at 300 K and then performed laser heating. The diffraction patterns were collected at every 10–15 GPa from 1400 to 2600 K up to 203 GPa. Assuming Graybody radiation, the temperature was determined by fitting the thermal radiation spectrum using the Planck radiation function (Prakapenka et al. 2008). Diffraction patterns were also collected at 300 K after each heating cycle at high pressures.

Results

The starting $CaSiO_3$ wollastonite became amorphous at 160 GPa and 300 K. Heating the amorphous material immediately transformed $CaSiO_3$ to the cubic perovskite structure (Fig. 1). Continuing heating cubic $CaSiO_3$-perovskite up to 2600 K did not cause any notable change in the XRD patterns. Yet the quenched sample at 300 K and 148 GPa has exhibited an obvious splitting

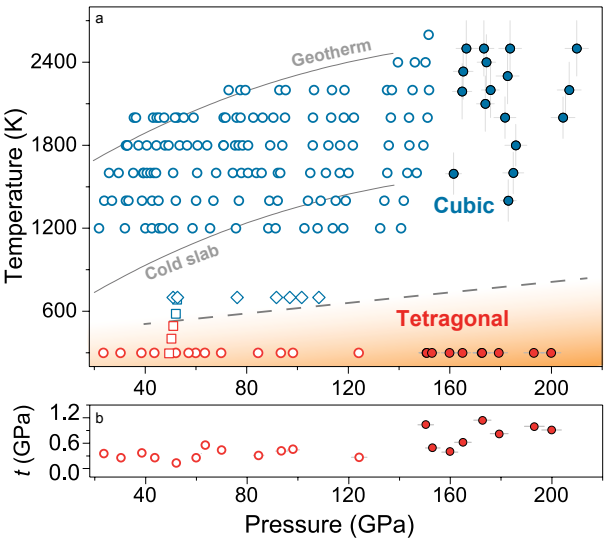

Figure 1. (**a**) Experimental pressure-temperature conditions of $CaSiO_3$-perovskite. Blue = cubic $CaSiO_3$-perovskite; red = tetragonal $CaSiO_3$-perovskite; solid circles = this study; open circles = Sun et al. (2016); diamonds = Noguchi et al. (2013); squares = Kurashina et al. (2004); gray lines = typical lower mantle geotherm and a representative cold slab geotherm, respectively (Brown and Shankland 1981; Kirby et al. 1996); dashed black lines = phase boundary between the cubic and tetragonal phases based on previous experimental results (Kurashina et al. 2004; Noguchi et al. 2013; Sun et al. 2016). (**b**) Calculated deviatoric stress (absolute value) at 300 K. Solid circles = this study; open circles = calculated using results in Sun et al. (2016). (Color online.)

of XRD peaks at 12.0°, 14.7°, and 16.9° (wavelength = 0.3344 Å), respectively. In particular, we observed a new peak at ~10.0–10.2° in the diffraction patterns after quench. The occurrence of the peak is consistent with the *I*4/*mcm* structure, which was not reported or not clearly identified in previous experimental studies (Fig. 2) (Chen et al. 2018; Ono et al. 2004; Shim et al. 2002; Thomson et al. 2019). Further analysis of the obtained XRD patterns revealed that $CaSiO_3$ was stable in the cubic perovskite structure between 158 and 203 GPa at 1400–2600 K but transformed to the tetragonal phase after quench. Calculated deviatoric stress at 300 K using collected diffraction patterns of Pt is less than 1.2 GPa at pressures up to 199 GPa (Fig. 1).

Here we focused on the lattice parameters and EoS of tetragonal $CaSiO_3$-perovskite (Fig. 3). Experimental data of Sun et al. (2016) between 24 and 124 GPa at 300 K have been re-analyzed to better constrain the lattice parameters and pressure-volume relationship of the tetragonal phase in an extended pressure range. For *I*4/*mcm*, *c*-axis is longer than *a*-axis (Table 1). The pressure-volume data were fitted using the Birch-Murnaghan EoS (Birch 1938) (Fig. 3; Table 2):

$$P = \frac{3}{2}K_{0T}\left[\left(\frac{V}{V_0}\right)^{-7/3} - \left(\frac{V}{V_0}\right)^{-5/3}\right] \cdot \left\{1 + \frac{3}{4}(K' - 4)\left[\left(\frac{V}{V_0}\right)^{-2/3} - 1\right]\right\}$$

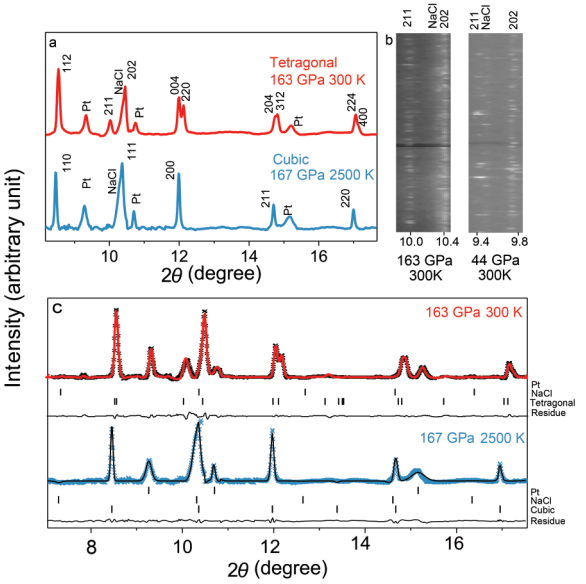

Figure 2. XRD patterns of $CaSiO_3$-perovskite at high pressures. (**a**) Representative XRD patterns of $CaSiO_3$-perovskite at high pressures and temperatures. Red line = cubic $CaSiO_3$-perovskite at 170 GPa and 2500 K; blue line = tetragonal $CaSiO_3$-perovskite at 163 GPa and 300 K. (**b**) Cake patterns of tetragonal $CaSiO_3$-perovskite at 163 and 44 GPa, respectively. The characteristic 211 peak at 2θ around 10° in the *I*4/*mcm* tetragonal phase is shown as a continuous ring; X-ray wavelength is 0.3344 Å. (Color online.)

Table 1. Pressure-volume data of tetragonal $CaSiO_3$-perovskite at high pressures and 300 K

P (GPa)	*a* (Å)	*c* (Å)	*V* (Å^3)
21.5(4)[a]	4.904(2)	6.947(3)	167.0(2)
24.9(6)[a]	4.882(3)	6.926(4)	165.1(3)
30.2(5)[a]	4.875(2)	6.920(3)	164.4(2)
38.4(7)[a]	4.837(1)	6.868(3)	160.7(1)
43.6(11)[a]	4.822(3)	6.823(5)	158.7(3)
52.0(13)[a]	4.776(2)	6.796(3)	155.0(2)
57.0(15)[a]	4.753(4)	6.747(5)	152.4(4)
59.9(15)[a]	4.743(2)	6.741(3)	151.7(2)
63.4(16)[a]	4.741(2)	6.731(3)	151.3(2)
69.9(17)[a]	4.717(3)	6.701(4)	149.1(3)
84.4(21)[a]	4.673(1)	6.651(2)	145.2(1)
93.4(24)[a]	4.643(2)	6.621(3)	142.7(2)
98.1(26)[a]	4.621(4)	6.585(5)	140.6(4)
124.0(30)[a]	4.565(3)	6.503(5)	135.5(3)
148.3(36)	4.502(3)	6.433(5)	130.4(3)
148.4(36)	4.500(3)	6.430(5)	130.2(3)
159.2(38)	4.481(2)	6.400(4)	128.5(2)
163.3(40)	4.471(2)	6.384(3)	127.6(2)
171.4(41)	4.460(2)	6.374(3)	126.8(2)
172.6(41)	4.461(1)	6.378(2)	126.9(1)
179.2(43)	4.449(3)	6.356(2)	125.8(2)
193.1(48)	4.428(3)	6.333(5)	124.2(3)
199.2(47)	4.415(2)	6.315(4)	123.1(2)

[a] Sun et al. (2016).

where K_{0T} and V_0 are the isothermal bulk modulus and unit-cell volume at the ambient conditions, respectively. K' is the pressure derivative of the bulk modulus. To have a better comparison with previous experimental and theoretical results, we normalized the *Z* number of the tetragonal phase to 1. In the normalized unit cell, *c* equals that of the tetragonal $CaSiO_3$-perovskite with $Z = 4$ divided by 2, while *a* equals the initial *a* divided by $\sqrt{2}$ (Chen et al. 2018; Jung and Oganov 2005; Ono et al. 2004; Shim et al. 2002). Here, with a free fitting of K', we obtained the modified $V_0 = 45.6(4)$ Å^3 ($Z = 1$), $K_{0T} = 227(21)$ GPa, and $K' = 4.0(3)$.

Discussion

Due to the similarity in the XRD patterns between the cubic and tetragonal $CaSiO_3$, the stable structure of $CaSiO_3$ at high-pressure-temperature conditions has been under debate for years (Chen et al. 2018; Jung and Oganov 2005; Ono et al. 2004; Shim et al. 2002; Stixrude et al. 2007). Splitting of the cubic 200 peak was applied to determine the occurrence of the phase transition at high pressures (Chen et al. 2018; Komabayashi et al. 2007; Kurashina et al. 2004; Noguchi et al. 2013; Ono et al. 2004; Shim et al. 2002; Sun et al. 2016). Here, our obtained XRD patterns above 148 GPa showed a well-resolved splitting of the cubic 200, 211, and 220 peaks after quench, while previous studies were not as clear or only observed several of them (Chen et al. 2018; Ono et al. 2004; Shim et al. 2002). Using the space groups and lattice parameters, we also calculated the full-width at half maximum (FWHM) values of the tetragonal 004+220, 204+312, and 224+400 peak pairs at high pressure and 300 K (Fig. 4). Across the cubic-tetragonal transition, the 200, 211, and 220 peaks of the cubic phase split into 004+220, 204+312, and

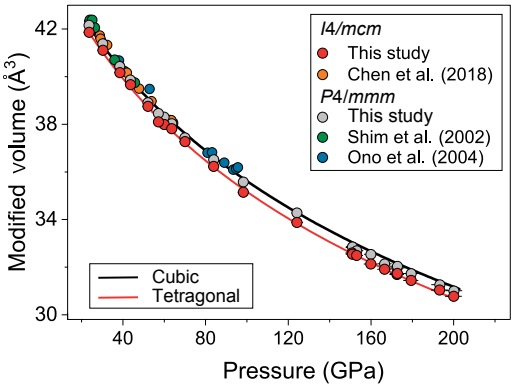

Figure 3. Pressure-volume relationship of tetragonal $CaSiO_3$-perovskite at high pressures and 300 K. Red circles and line = the *I*4/*mcm* phase in this study; green circles = the *P*4/*mmm* phase (Shim et al. 2002); blue circles = the *P*4/*mmm* phase (Ono et al. 2004); orange circles = the *I*4/*mcm* phase (Chen et al. 2018); gray circles = this study assuming a *P*4/*mmm* tetragonal structure; black lines = calculated volume of the cubic $CaSiO_3$-perovskite at 300 K (Sun et al. 2016). (Color online.)

Table 2. EoS of the tetragonal $CaSiO_3$-perovskite under self-consistent pressure scales

	This study	This study	Shim (2002)	Ono (2004)	Chen (2018)	Thomson (2019)	Jung (2005)[b]	Stixrude (2007)[b]	Caracas (2005)[b]
K_{0T} (GPa)	227(21)	229(4)	259(5)	235(9)	228(6)	224(4)	219.04	252	249
K'	4.0(3)	4[a]	4[a]	4[a]	4[a]	4[a]	4.08	4.1	4.09
V_0 (Å^3)	45.6(4)	45.6(2)	45.58[f]	45.9(4)	46.2(1)	46.10(6)	46.89	44.00	44.537

[a] Fixed.
[b] Theoretical results, at 0 K.

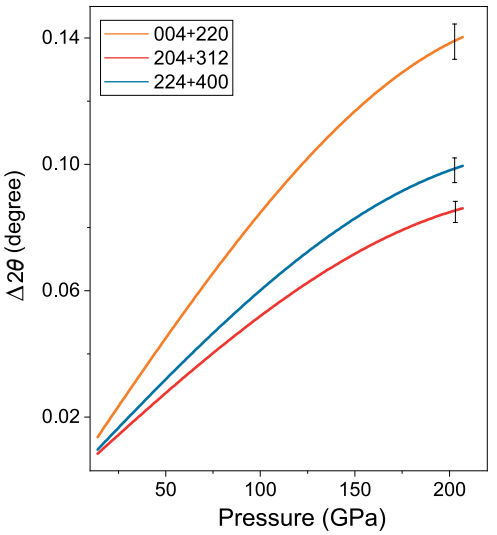

Figure 4. Modeled peak widths of the tetragonal phase at high pressures. Orange = tetragonal peaks 004+220 from splitting of the cubic 200 peak after quench; red = tetragonal peaks 204+312 from splitting of the cubic 211 peak after quench; blue = tetragonal peak 224+400 s from splitting of the cubic 220 peak after quench. (Color online.)

224+400 peaks, respectively, in the tetragonal phase. The FWHM values of the peak pairs in the tetragonal structure exhibit a substantial increase with pressure up to 200 GPa. It is thus easier to identify the presence of tetragonal $CaSiO_3$-perovskite from the XRD patterns at pressures above 148 GPa, but also make the fitting of volume and lattice parameter more accurate. Previous studies mentioned that the observed peak splitting may be a result of the increased deviatoric stress inside the DAC, and a deviatoric stress of ~7 GPa is enough to induce the peak splitting at temperatures as high as 1550 K (Chen et al. 2018; Shim et al. 2002). Here we showed that the diffraction patterns after quench have a deviatoric stress less than 1.2 GPa up to 199 GPa (Singh, 1993; Sun et al. 2016) (Fig. 1). The peak splitting in the quenched sample can only be caused by the phase transition but not by the deviatoric stress (Chen et al. 2018; Shim et al. 2002).

More importantly, we have observed the presence of an additional peak with 2θ at ~10.0–10.2° from 148 to 199 GPa at 300 K (*d*-spacing of 1.92–1.88 Å) (Fig. 2). Among four potential structures, this peak with 2θ at ~10.0–10.2° assigned as reflection 211 in the tetragonal structure can only be explained by *I*4/*mcm*, but was not observed in previous experimental work (Chen et al. 2018; Ono et al. 2004; Shim et al. 2002). Although Sun et al. (2016) did observe the 211 peak, their motivation was to determine the thermal EoS of cubic $CaSiO_3$-perovskite. We also examined the XRD patterns of tetragonal $CaSiO_3$-perovskite in Sun et al. (2016) between 24 and 124 GPa at 300 K, which also recorded the tetragonal 211 peak as a continuous ring (Fig. 2). Rotation of the sample when collecting the XRD patterns helped reveal the 211 peak more clearly as a relatively continuous ring in the cake patterns (Fig. 2) (Ma et al. 2004; Smith and Desgreniers 2009). The presence of peak 211 is a new indicator for the cubic to tetragonal phase transition and provides an additional constraint on the lattice parameter *a* and *c*. From the obtained XRD patterns, *a*-axis of the tetragonal *I*4/*mcm* phase is calculated to be ~2.5% shorter than that of the cubic phase because of the structural distortion. With $Z = 1$, previous experimental studies reported a modified *c*/*a* value less than 1 for the *P*4/*mmm* phase (Fig. 5) (Chen et al. 2018; Jung and Oganov 2005; Ono et al. 2004; Shim et al. 2002; Stixrude et al. 2007). For the *I*4/*mcm* structure, *c*-axis is longer than *a*-axis, leading to a modified *c*/*a* ratio greater than 1. The modified *c*/*a* ratio of the tetragonal $CaSiO_3$-perovskite increases from ~1.003 at 24 GPa to ~1.012 at 199 GPa (Fig. 5). The modified *c*/*a* ratios obtained in this work between 24 and 199 GPa are in general agreement with a recent experimental study and follow a similar trend with pressure as the theoretical predictions (Chen et al. 2018; Stixrude et al. 2007).

The unit-cell volume of the *I*4/*mcm* phase at a given pressure shown here is slightly smaller than that reported in previous studies using the *P*4/*mmm* structure (Ono et al. 2004; Shim et al. 2002). The difference is caused by using different sequence of peaks in two space groups to analyze the XRD pattern. If the *P*4/*mmm* structure is used to calculate the unit-cell volume of the tetragonal $CaSiO_3$ by neglecting the 211 peak, the calculated volume is similar to that shown in previous studies (Fig. 3) (Ono et al. 2004; Shim et al. 2002). Above 45 GPa, the unit cell volumes of the *P*4/*mmm* structure in Ono et al. (2004) are greater than other results, potentially due to large deviatoric stress with no pressure medium used in the high-pressure experiments (Chen et al. 2018; Shim et al. 2002;

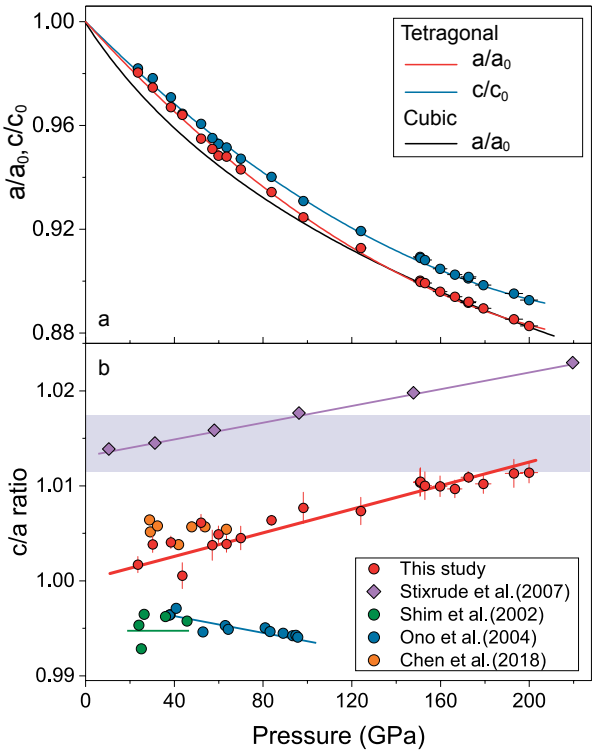

Figure 5. Lattice parameters of tetragonal $CaSiO_3$-perovskite. (**a**) Variation of *a*- and *c*-axis of tetragonal $CaSiO_3$-perovskite with pressure at 300 K. Blue = *c*-axis; red = *a*-axis. (**b**) The modified *c*/*a* ratios of tetragonal $CaSiO_3$-perovskite at high pressures and 300 K. Red = this study; green = Shim et al. (2002); blue = Ono et al. (2004); orange = Chen et al. (2018); purple = Stixrude et al. (2007). (Color online.)

Thomson et al. 2019). K_{0T} of the tetragonal $CaSiO_3$-perovskite with a fixed $K'_{0T} = 4$ is highly uncertain, ranging from 223(6) to 248(8) GPa in previous experimental studies (Chen et al. 2018; Gréaux et al. 2019; Ono et al. 2004; Shim et al. 2002; Thomson et al. 2019). Here, fitting the *P-V* data in a much larger pressure range up to 200 GPa yielded K_{0T} of 227(21) with a free K'. For a better comparison, we re-analyzed the previous experimental *P-V* data using a self-consistent pressure scale of Fei et al. (2007) (Table 2; Shim et al. 2002; Ono et al. 2004; Chen et al. 2018; Thomson et al. 2019; Jung and Oganov 2005; Stixrude et al. 2007; Caracas et al. 2005). Previous experimental studies with a much lower K_{0T} could be caused by a limited experimental pressure range at 300 K or the untransformed lower-pressure materials (Chen et al. 2018; Ono et al. 2004; Thomson et al. 2019; Gréaux et al. 2019). K_{0T} of the tetragonal phase in Shim et al. (2002) is much greater than our and other literature results, potentially due to their limited experimental data points and narrow pressure range (Chen et al. 2018; Ono et al. 2004). In addition, tetragonal $CaSiO_3$-perovskite has a slightly lower K_{0T} than the cubic phase, although a few experimental studies reported a low K_{0T} of 208–237 GPa for the cubic phase (Gréaux et al. 2019; Kawai and Tsuchiya 2014; Noguchi et al. 2013; Ricolleau et al. 2009; Shim et al. 2000, 2002; Wang et al. 1996; Zhang et al. 2006).

Geophysical implications

A recent experimental study showed that addition of Ti in $CaSiO_3$-perovskite could elevate the phase transition temperature from the cubic to the tetragonal phase (Thomson et al. 2019). Ti-bearing tetragonal $CaSiO_3$-perovskite may exist in the cold subducting slabs in the Earth's lower mantle (Ono et al. 2004; Thomson et al. 2019). Here we modeled the sound velocities of tetragonal and cubic end-member $CaSiO_3$-perovskites using our obtained EoS together with literature results (Fig. 6) (Gréaux et al. 2019; Thomson et al. 2019). Because of the second-order transition, the density of the tetragonal $CaSiO_3$-perovskite along the phase boundary will be the same as the cubic phase. The phase boundary between the tetragonal and cubic $CaSiO_3$-perovskites was only determined at ~50 GPa and 580 K by Kurashina et al. (2004). Here we modeled the velocity change across the phase transition at 580 K between 40 and 60 GPa. Using the estimated Clapeyron slope in Kurashina et al. (2004), the tetragonal to cubic phase transition temperature is estimated to be ~1000 K between 100 and 120 GPa. The velocity change across the phase transition between 100 and 120 GPa was also shown in Figure 6. For the cubic phase, Thomson et al. (2019) and Gréaux et al. (2019) reported different bulk and shear moduli as well as their pressure and temperature derivatives. Both of their results were used to calculate the sound velocities of the cubic phase. The obtained K_{0T}, K', and V_0 in this study, together with necessary parameters in Thomson et al. (2019) and Gréaux et al. (2019), were used to calculate the velocity of the tetragonal phase. Due to the lack of experimental constraints, some thermoelastic parameters of tetragonal $CaSiO_3$-perovskite, such as dK/dT and dG/dT, were assumed to be the same as the cubic phase (Thomson et al. 2019; Gréaux et al. 2019). Uncertainties of the calculated sound velocities because of using different literature elastic parameters were shown in shading in Figure 6 (Gréaux et al. 2019; Thomson et al. 2019).

The compressional (V_P) and shear-wave velocities (V_S) of tetragonal $CaSiO_3$-perovskite are ~5.3% and ~6.7% lower than those of the cubic phase at ~50 GPa and 580 K, respectively (Fig. 6). At 1000 K and 100 GPa, the difference in V_P and V_S between the cubic and tetragonal phases is ~4.3% and ~9.1%, respectively. In the subducted oceanic crust, the volume percentage of $CaSiO_3$-perovskite could be as great as 22–29% (e.g., Anderson 1989; Harte 2010; Hirose et al. 2005; Wood 2000). The velocity jump caused by the tetragonal to cubic phase transition in $CaSiO_3$-perovskite will be 1.3% in V_P and 1.7% in V_S at ~50 GPa, and 1.1% in V_P and 2.3% in V_S at ~110 GPa in the cold subduction oceanic crust. Without experimental constraints on the influence of Ti on the phase boundary and thermal elastic properties of the tetragonal and cubic phases, our modeling can only provide a preliminary estimation on the influence of the phase transition of $CaSiO_3$ on the velocity profiles of the lower mantle.

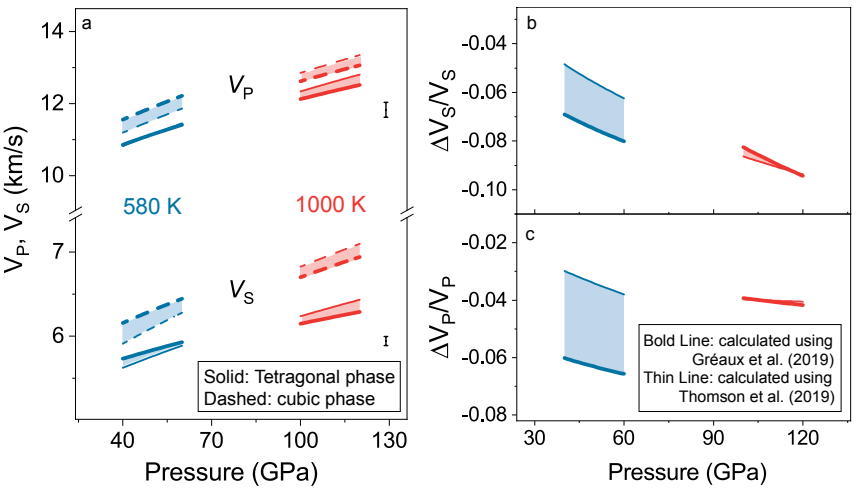

Figure 6. Modeled compressional (V_P) and shear-wave velocities (V_S) of $CaSiO_3$-perovskite at ~50 and 110 GPa. (**a**) Calculated velocities at 580 K between 40 and 60 GPa and at 1000 K between 100 and 120 GPa; solid lines = tetragonal phase; dashed lines = cubic phase; blue = V_S and V_P at 580 K; red = V_S and V_P at 1000 K; bold lines = calculated using results from this work and Gréaux et al. (2019); thin lines = calculated using results from this work and Thomson et al. (2019). (**b**) The shear-wave velocity change ΔV_S aross the tetragonal to cubic phase transition. (**c**) The compressional-wave velocity change ΔV_P aross the tetragonal to cubic phase transition; bold lines = calculated using results from this work and Gréaux et al. (2019); thin lines = calculated using results from this work and Thomson et al. (2019). Density was assumed to be the same for both tetragonal and cubic phases due to the second-order phase transition. Vertical ticks represent the calculation errors using standard error propagation from the used parameters. (Color online.)

In summary, the structure of $CaSiO_3$ has been studied up to 200 GPa by synchrotron XRD in laser-heated DACs. Quenching to 300 K leads to the transition of $CaSiO_3$ from the cubic to the tetragonal structure. Compared to previous experimental results, here we have observed more distinct splittings of the cubic 200, 211, and 220 peaks after temperature quench between 148 and 199 GPa. The new peak 211 with 2θ around 10.0–10.2° is consistent with the *I*4/*mcm* structure. We note that the *I*4/*mcm* tetragonal phase has a modified *c*/*a* ratio ($Z = 1$) >1, which increases from 1.002 at ~20 GPa to 1.012 at ~200 GPa. The obtained K_{0T} of the *I*4/*mcm* phase is smaller than that of the cubic $CaSiO_3$-perovskite. The comparison in V_P and V_S between tetragonal and cubic $CaSiO_3$-perovskites at high temperature and pressure is useful to estimate the influence of the phase transition on the velocity profiles of the lower mantle, indicating the phase transition can cause a substantial increase in the sound velocity. Future studies are expected to determine the effect of Ti on the thermoelastic parameters of tetragonal $CaSiO_3$-perovskite and provide new insights into the composition and structure of the lower mantle.

Funding

Z. Mao acknowledges supports from the National Science Foundation of China (41874101), Strategic Priority Research Program of the Chinese Academy of Sciences (XDB41000000), National Key R&D Program of China (2018YFA0702703), and Funds for leading talents of USTC (KY2080000061). N. Sun acknowledges supports from Fundamental Research Funds for the Central Universities (WK2080000133). J.F. Lin acknowledges support from Geophysics Program of the National Science Foundation (EAR-1916941). Portions of this work were performed at GeoSoilEnviroCARS (The University of Chicago, Sector 13), Advanced Photon Source (APS), Argonne National Laboratory. GeoSoilEnviroCARS is supported by the National Science Foundation-Earth Sciences (EAR-1634415) and Department of Energy-GeoSciences (DE-FG02-94ER14466). This research used resources of the Advanced Photon Source, a U.S. Department of Energy (DOE) Office of Science User Facility operated for the DOE Office of Science by Argonne National Laboratory under Contract No. DE-AC02-06CH11357.

References cited

Akber-Knutson, S., Bukowinski, M.S.T., and Matas, J. (2002) On the structure and compressibility of $CaSiO_3$ perovskite. Geophysical Research Letters, 29.

Anderson, D.L. (1989) Theory of the Earth. Oxford, Blackwell Scientific Publications.

Birch, F. (1938) The effect of pressure upon the elastic parameters of isotropic solids, according to Murnaghan's theory of finite strain. Journal of Applied Physics, 9, 279–288.

Caracas, R., Wentzcovitch, R., Price, G.D., and Brodholt, J. (2005) $CaSiO_3$ perovskite at lower mantle pressures. Geophysical Research Letters, 32.

Chen, H., Shim, S., Leinenweber, K., Prakapenka, V., Meng, Y., and Prescher, C. (2018) Crystal structure of $CaSiO_3$ perovskite at 28–62 GPa and 300 K under quasi-hydrostatic stress conditions. American Mineralogist, 103, 462–468.

Dziewonski, A.M., and Anderson, D.L. (1981) Preliminary Reference Earth Model. Physics of the Earth and Planetary Interiors, 25, 297–356.

Fei, Y.W., Ricolleau, A., Frank, M., Mibe, K., Shen, G.Y., and Prakapenka, V. (2007) Toward an internally consistent pressure scale. Proceedings of the National Academy of Sciences, 104, 9182–9186.

Gréaux, S., Irifune, T., Higo, Y., Tange, Y., Arimoto, T., Liu, Z.D., and Yamada, A. (2019) Sound velocity of $CaSiO_3$ perovskite suggests the presence of basaltic crust in the Earth's lower mantle. Nature, 565, 218–221.

Harte, B. (2010) Diamond formation in the deep mantle: The record of mineral inclusions and their distribution in relation to mantle dehydration zones. Mineralogical Magazine, 74, 189–215.

Hirose, K., and Fei, Y.W. (2002) Subsolidus and melting phase relations of basaltic composition in the uppermost lower mantle. Geochimica et Cosmochimica Acta, 66, 2099–2108.

Hirose, K., Takafuji, N., Sata, N., and Ohishi, Y. (2005) Phase transition and density of subducted MORB crust in the lower mantle. Earth and Planetary Science Letters, 237, 239–251.

Jung, D.Y., and Oganov, A.R. (2005) Ab initio study of the high-pressure behavior of $CaSiO_3$ perovskite. Physics and Chemistry of Minerals, 32, 146–153.

Kawai, K., and Tsuchiya, T. (2014) *P-V-T* equation of state of cubic $CaSiO_3$ perovskite from first-principles computation. Journal of Geophysical Research: Solid Earth, 119, 2801–2809.

Kesson, S.E., Fitz Gerald, J.D., and Shelley, J.M.G. (1994) Mineral chemistry and density subducted basaltic crust at lower-mantle pressures. Nature, 372, 767–769.

——— (1998) Mineralogy and dynamics of a pyrolite lower mantle. Nature, 393, 252–255.

Komabayashi, T., Hirose, K., Sata, N., Ohishi, Y., and Dubrovinsky, L.S. (2007) Phase transition in $CaSiO_3$ perovskite. Earth and Planetary Science Letters, 260, 564–569.

Kudo, Y., Hirose, K., Murakami, M., Asahara, Y., Ozawa, H., Ohishi, Y., and Hirao, N. (2012) Sound velocity measurements of $CaSiO_3$ perovskite to 133 GPa and implications for lowermost mantle seismic anomalies. Earth and Planetary Science Letters, 349-350, 1–7.

Kurashina, T., Hirose, K., Ono, S., Sata, N., and Ohishi, Y. (2004) Phase transition in Al-bearing $CaSiO_3$ perovskite: implications for seismic discontinuities in the lower mantle. Physics of the Earth and Planetary Interiors, 145, 67–74.

Li, L., Weidner, D.J., Brodholt, J., Alfe, D., Price, G.D., Caracas, R., and Wentzcovitch, R. (2006) Phase stability of $CaSiO_3$ perovskite at high pressure and temperature: Insights from ab initio molecular dynamics. Physics of the Earth and Planetary Interiors, 155, 260–268.

Ma, Y.Z., Somayazulu, M., Shen, G.Y., Mao, H.K., Shu, J.F., and Hemley, R.J. (2004) In situ X-ray diffraction studies of iron to Earth-core conditions. Physics of the Earth and Planetary Interiors, 143-144, 455–467.

Magyari-Köpe, B., Vitos, L., Grimvall, G., Johansson, B., and Kollár, J. (2002) Low-temperature crystal structure of $CaSiO_3$ perovskite: An ab initio total energy study. Physical Review B, 65.

Mao, H.K., Chen, L.C., Hemley, R.J., Jephcoat, A.P., Wu, Y., and Bassett, W.A. (1989) Stability and Equation of State of $CaSiO_3$-perovskite to 134 GPa. Journal of Geophysical Research, 94, 17889–17894.

Murakami, M., Hirose, K., Sata, N., and Ohishi, Y. (2005) Post-perovskite phase transition and mineral chemistry in the pyrolitic lowermost mantle. Geophysical Research Letters, 32. doi:10.1029/2004GL021956.

Nestola, F., Korolev, N., Kopylova, M., Rotiroti, N., Pearson, D.G., Pamato, M.G., Alvaro, M., Peruzzo, L., Gurney, J.J., Moore, A.E., and Davidson, J. (2018) $CaSiO_3$ perovskite in diamond indicates the recycling of oceanic crust into the lower mantle. Nature, 555, 237–241.

Noguchi, M., Komabayashi, T., Hirose, K., and Ohishi, Y. (2013) High-temperature compression experiments of $CaSiO_3$ perovskite to lowermost mantle conditions and its thermal equation of state. Physics and Chemistry of Minerals, 40, 81–91.

Ono, S., Ohishi, Y., and Mibe, K. (2004) Phase transition of Ca-perovskite and stability of Al-bearing Mg-perovskite in the lower mantle. American Mineralogist, 89, 1480–1485.

Prakapenka, V.B., Kubo, A., Kuznetsov, A., Laskin, A., Shkurikhin, O., Dera, P., Rivers, M.L., and Sutton, S.R. (2008) Advanced flat top laser heating system for high pressure research at GSECARS: application to the melting behavior of germanium. High Pressure Research, 28, 225–235.

Ricolleau, A., Fei, Y.W., Cottrell, E., Watson, H., Deng, L.W., Zhang, L., Fiquet, G., Auzende, A.L., Roskosz, M., Morard, G., and Prakapenka, V. (2009) Density profile of pyrolite under the lower mantle conditions. Geophysical Research Letters, 36.

Ringwood, A.E. (1975) Composition and Petrology of the Earth's Mantle. xvi, 618 p. McGraw-Hill.

Shim, S.H., Duffy, T.S., and Shen, G.Y. (2000) The stability and *P-V-T* equation of state of $CaSiO_3$ perovskite in the Earth's lower mantle. Journal of Geophysical Research: Solid Earth, 105, 25955–25968.

Shim, S.H., Jeanloz, R., and Duffy, T.S. (2002) Tetragonal structure of $CaSiO_3$ perovskite above 20 GPa. Geophysical Research Letters, 29, 19-1–19-4.

Smith, J.S., and Desgreniers, S. (2009) Selected techniques in diamond anvil cell crystallography: centring samples using X-ray transmission and rocking powder samples to improve X-ray diffraction image quality. Journal of Synchrotron Radiation, 16, 83–96.

Stixrude, L., Lithgow-Bertelloni, C., Kiefer, B., and Fumagalli, P. (2007) Phase stability and shear softening in $CaSiO_3$ perovskite at high pressure. Physical Review B, 75.

Sun, N.Y., Mao, Z., Yan, S., Wu, X., Prakapenka, V.B., and Lin, J.F. (2016) Confirming a pyrolitic lower mantle using self-consistent pressure scales and new constraints on $CaSiO_3$ perovskite. Journal of Geophysical Research: Solid Earth, 121, 4876–4894.

Thomson, A., Crichton, W., Brodholt, J., Wood, J., Siersch, N., Muir, J., Dobson, D.P., and Hunt, S. (2019) Seismic velocities of $CaSiO_3$ perovskite can explain LLSVPs in Earth's lower mantle. Nature, 572, 643–647.

Wang, Y.B., Weidner, D.J., and Guyot, F. (1996) Thermal equation of state of $CaSiO_3$ perovskite. Journal of Geophysical Research: Solid Earth, 101, 661–672.

Wood, B.J. (2000) Phase transformations and partitioning relations in peridotite under lower mantle conditions. Earth and Planetary Science Letters, 174, 341–354.

Zhang, Y.G., Zhao, D.P., Matsui, M., and Guo, G.J. (2006) Equations of state of $CaSiO_3$ perovskite: A Molecular Dynamics study. Physics and Chemistry of Minerals, 33, 126–137.

Manuscript received November 29, 2020
Manuscript accepted January 15, 2021
Manuscript handled by Zhicheng Jing